Available online at www.sciencedirect.com
SCIENCE DIRECT®
Journal of Solid State Chemistry 177 (2004) 3616–3625
JOURNAL OF SOLID STATE CHEMISTRY
http://elsevier.com/locate/jssc

2D metal slabs in new nickel–tin chalcogenides $Ni_{7-\delta}SnQ_2$ (Q=Se, Te): average crystal and electronic structures, chemical bonding and physical properties

A.I. Baranov,[a] A.A. Isaeva,[a] L. Kloo,[b] V.A. Kulbachinskii,[c] R.A. Lunin,[c] V.N. Nikiforov,[c] and B.A. Popovkin[d,*]

[a] *Department of Materials Science, Moscow State University, Leninskie Gory, Moscow, 119992, GSP-2, Russia*
[b] *Inorganic Chemistry, Royal Institute of Technology, Stockholm, S 100 44, Sweden*
[c] *Department of Physics, Moscow State University, Leninskie Gory, Moscow, 119992, GSP-2, Russia*
[d] *Department of Chemistry, Moscow State University, Leninskie Gory, Moscow 119992, GSP-2, Russia*

Received 17 March 2004; received in revised form 26 May 2004; accepted 30 May 2004

Available online 21 August 2004

Abstract

A systematic search for mixed low-valence, nickel–tin chalcogenides performed by establishing phase relations in the parts of Ni–Sn–Se and Ni–Sn–Te ternary systems resulted in the discovery of two new compounds, $Ni_{5.62}SnSe_2$ and $Ni_{5.78}SnTe_2$. Single crystals of both compounds were prepared by chemical transport with iodine and crystal structures were determined by single crystal X-ray investigation. The ED patterns for $Ni_{5.78}SnTe_2$ showed the presence of satellite reflections, which indicate a modulated structure with $q \approx 0.4a^*$. Average crystal structures of both compounds were determined to be of tetragonal symmetry (Sp.gr. $I4/mmm$, $Z=2$) with $a=3.6890(8)$ Å, $c=18.648(3)$ Å, $R_w=0.0716$ and $a=3.7680(5)$ Å, $c=19.419(4)$ Å, $R_w=0.0832$, correspondingly, and are isostructural to known $Ni_{5.72}SbSe_2$ and $Ni_{5.66}SbTe_2$. Measurements were carried out for both compounds with respect to thermal, electrical and magnetic properties. Ab initio band structure calculations were also performed to take a first glance into the electronic structure of such type compounds. The anisotropy of their band structure was found. Physical property measurements showed both compounds to be the anisotropic metallic conductors and paramagnetics. Calculated difference charge density maps revealed pairwise covalent and multicenter metallic nature of the d-metal—chalcogen and d-metal—p-metal interactions, respectively.

Keywords: Heterometallic bonds; Mixed chalcogenides; Chemical bonding; Physical properties

1. Introduction

Recently, a new family of mixed metal-rich chalcogenides of nickel–antimony and nickel–tin was discovered. The crystal structures of $Ni_{5.72}SbSe_2$, $Ni_{5.66}SbTe_2$ [1] and Ni_6SnS_2 [2] are made by alternating bimetallic $^2_\infty[Ni_5M]$ (M=Sn, Sb) and nickel-chalcogenide $^2_\infty[Ni_xQ_2]$ (Q=S, $x=1$; Q=Se, $x=0.72$; Q=Te, $x=0.66$) slabs. In the $^2_\infty[Ni_5M]$ (M =Sn, Sb) slabs atoms are arranged in a Cu_3Au motif and in $^2_\infty[Ni_xQ_2]$ slabs atoms are arranged either in NaCl (Q=S, Se, Te) or in Li_2O (Q=S) motifs. The crystal structure of $Ni_9Sn_2S_2$ [2] contains double-stacked $^2_\infty[Ni_5Sn]$ slabs of formal composition $^2_\infty[Ni_8Sn_2]$ and two types of $^2_\infty[NiS_2]$ slabs of NaCl and Li_2O type. Quantum-chemical calculations performed for the nickel–tin sulfides [2] revealed different nature of chemical bonding within the bimetallic and nickel–sulfide slabs, which turned out to be multicenter, metal-like in the former and classical pairwise in the latter. The dependence of resistivity on temperature was measured on pressed powder samples [1]. However, disregarding the anisotropic nature of the compounds, no anisotropy was observed experimentally on their physical properties.

*Corresponding author. Fax: +7-095-939-0171.
E-mail address: popovkin@inorg.chem.msu.ru (B.A. Popovkin).

0022-4596/$ - see front matter © 2004 Elsevier Inc. All rights reserved.
doi:10.1016/j.jssc.2004.05.061

The fact that various nickel-*p*-metal and nickel-chalcogenide slabs can be combined producing different crystal structures suggests that other compounds of such type can be obtained. The goals of the present work were the systematic search for metal-rich, nickel–tin selenides and tellurides, the investigation of their crystal and electronic structures, as well as physical properties.

2. Experimental

2.1. Study of phase relations

About 10 samples having compositions in the metal-rich parts of the Ni–Sn–*Q* (*Q*=Se, Te) ternary systems were studied for each system. The appropriate mixtures of the elements (all of 99.99% purity powders,[1] 1 g total) were loaded into silica ampoules, evacuated (10^{-2} mm Hg), and sealed. The total annealing time (540°C, with several intermediate grindings in an agate mortar and reannealings of products pressed into pellets) was about 10–20 days depending on whether the equilibrium had been reached. The phase composition of the annealed samples was studied by X-ray powder diffraction [Cu$K\alpha_1$, STADI/P diffractometer (Stoe)]. The maximum number of phases found in each sample was equal to 3, thus confirming the equilibrium state reached. The existence of two new ternary phases, $Ni_{5.62}SnSe_2$ and $Ni_{5.78}SnTe_2$, was observed. The isothermal phase relation schemes established for each Ni–Sn–*Q* (*Q*=Se, Te) system are presented in Fig. 1. The composition of each compound was revealed by means of single crystal X-ray diffraction and EDX analysis (see below).

The single crystals of the title compounds were prepared from the vapor phase by means of chemical transport reaction with I_2 in 16×100 mm silica ampoules placed in a horizontal, two-temperature furnace. Pre-annealed charges of the total mass of about 0.25 g were used. Other conditions of the crystal growth experiments are specified in Table 1. The formation of crystals was observed in the cold part of the ampoules.

2.2. Synthesis

The stoichoimetric mixtures of the elements were annealed in evacuated silica ampoules at 540°C for 7 days. The products were then ground in an agate mortar, pressed into pellets and further reannealed under the same conditions several times (2 for $Ni_{5.62}SnSe_2$ and 4 for $Ni_{5.78}SnTe_2$). The grayish powders obtained were identified by powder X-ray diffraction [Cu$K\alpha_1$, STADI/P diffractometer (Stoe)], which showed

[1] Ni powder as received was preheated at 500°C in a flow of hydrogen during 3h in order to remove nickel oxide impurities.

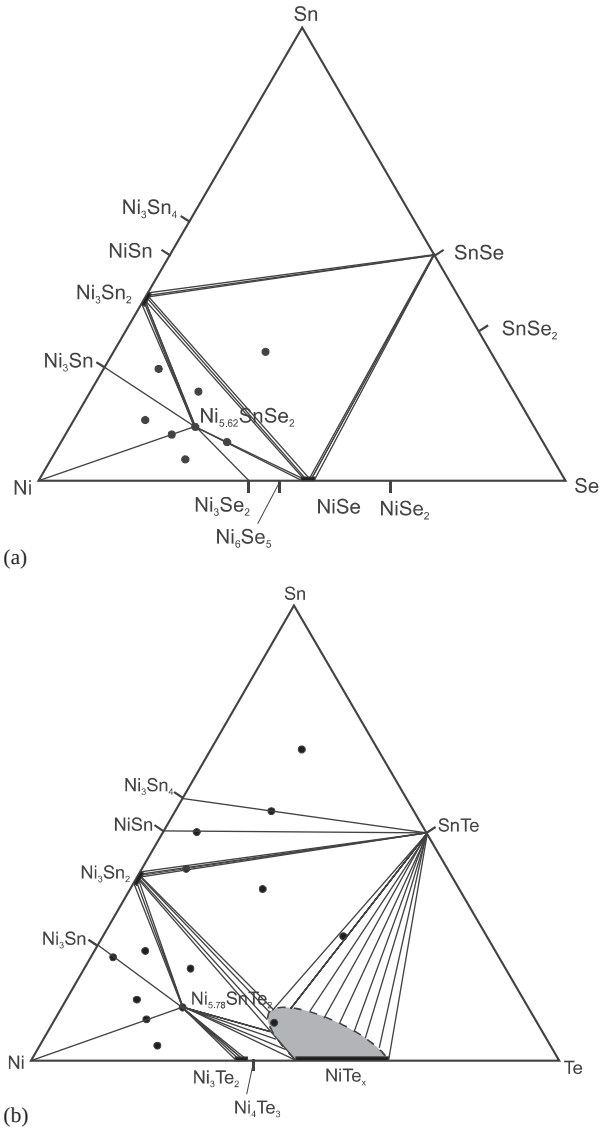

Fig. 1. Phase equillibria in the Ni–Sn–Se (a) and Ni–Sn–Te (b) system at 540°C. Black dots correspond to synthesized samples. Binary phases are according to Lyakishev [3]. The boundary of the $NiTe_x$-based solid solution is only approximate.

almost complete agreement with the theoretical patterns of $Ni_{5.62}SnSe_2$ and $Ni_{5.78}SnTe_2$ generated from the single crystal X-ray diffraction data (see below). Additional weak peaks were observed in each diffractogram (Guinier camera Enraf-Nonius FR-552), which cannot be assigned to any impurity phase, or trivial superstructures. The substances are stable in air for several months. $Ni_{5.62}SnSe_2$ is stable in diluted hydrochloric acid, while $Ni_{5.78}SnTe_2$ slowly dissolves in warm HCl. Both compounds dissolve readily in nitric acid.

2.3. Crystal structure determination

X-ray single crystal diffraction data were recorded on Bruker-Nonius KappaCCD diffractometer (Ag$K\alpha_1$

Table 1
Crystal growth conditions and results

	$Ni_{5.62}SnSe_2$	$Ni_{5.78}SnTe_2$
Initial composition of charge	60Ni + 9Sn + 31Se	11Ni + 2Sn + 2Te
Phase composition of charge and annealing conditions	$Ni_{5.62}SnSe_2$ + NiSe (540°C, 16 days)	$Ni_{5.78}SnTe_2$ + Ni_3Sn (600°C, 24 days)
I_2 concentration (mol/L)	0.004	0.002
$T_{charge}/T_{empty\ end}$ (°C)	600/550	620/550
Growth time (days)	14	10

Table 2
Crystal structure determination of $Ni_{7-\delta}SnQ_2$ (Q = Se,Te)

Formula	$Ni_{5.62(1)}SnSe_2$	$Ni_{5.78(2)}SnTe_2$
Space group	$I4/mmm$ (No. 139)	$I4/mmm$ (No. 139)
a (Å)	3.6890(8)	3.7680(5)
c (Å)	18.648(3)	19.419(4)
V (Å^3)	253.78(9)	275.71(8)
Z	2	2
θ_{max} (deg)	27.83	26.89
θ_{step} (deg/frame)	1	1
Collection time (s/frame)	40	40
ρ_{calc} (g cm^{-3})	7.942	8.581
μ (mm^{-1})	20.693	17.780
Crystals shape, color and size	Silver plates, 0.2 × 0.2 × 0.01 mm	Dark bricks, 0.1 × 0.05 × 0.15 mm
GoF, all data	1.044	1.076
largest diff. peak and hole (e Å^{-3})	4.430 and –2.770	2.615 and –2.816
measd refln/independ refln/parameters	595/226/17	314/221/16
$R(F)$ for $F_o^2 > 4\sigma(F_o^2)$[a]	0.0415	0.0384
$R_w(F_o^2)$	0.0716	0.0832
W	$1/[\sigma^2(F_o^2) + (0.0206P)^2]$[b]	$1/[\sigma^2(F_o^2) + (0.0412P)^2]$[b]

[a] $-R(F) = \{\sum||F_o| - |F_c||\}/\{\sum|F_o|\}$.
[b] $- P = (F_o^2 + 2F_c^2)/3$.

radiation, $\lambda = 0.56090$ Å, graphite monochromator). The data sets were collected at the ambient temperature with the data collection parameters and results listed in Table 2. An analysis of the data collected is consistent with the tetragonal crystal system with the only systematic extinctions corresponding to an I-centered cell. The space group $I4/mmm$ (No. 139) was chosen for the structure solution. The positions of heavy atoms (Te, Se, Sn) were found with the Patterson function (SHELXS-97 [4]). Nickel atoms were localized by a sequence of least-square refinement and $\Delta\rho(x, y, z)$ synthesis (SHELXL-97 [4]). Semiempirical absorption corrections (SCALE-PACK software [5]) were applied. One of the Ni sites in each crystal structure was refined with a fractional occupation. Positional parameters are listed in Table 3. Further details of the crystal structure investigations can be obtained from the Fachinformationszentrum Karlsruhe, 76344 Eggenstein-Leopoldshafen, Germany, (fax: +497247-808-666, mail to: crysdata@fiz.karlsruhe.de) on quoting the depository numbers CSD413861 and CSD413862. The compositions $Ni_{5.62}SnSe_2$ and $Ni_{5.78}SnTe_2$ were verified by EDX analysis.[2]

To find out the nature of above-mentioned extra lines observed on experimental powder patterns of $Ni_{5.78}SnTe_2$, additional ED experiments were undertaken. Samples for the ED study were prepared by grinding the single crystals in ethyl alcohol with agate mortar and deposing fragments on a holey carbon grid. ED patterns were obtained in a JEM-2000FXII electron microscope.

Attempts were made to obtain the derivative compounds of composition Ni_6SnQ_2 and Ni_7SnQ_2 (Q=Se, Te), which might possess the same crystal structures but with the Ni(3) site occupation equal to 1/2 or 1, correspondingly. Samples were synthesized at 540°C (1000 h, 2 intermediate grindings followed by pressing into pellets and further annealing). X-ray powder

[2] CAMEBAX SX-50, acc. voltage 15 kV, coll. time 100 s, calculated (at %.): 65.2 Ni, 11.6 Sn, 23.2 Se and 65.7 Ni, 11.4 Sn, 22.8 Te; found: 64.7 Ni 11.9 Sn 22.9 Se and 64.6 Ni 11.8 Sn 23.4 Te.

Table 3
Positional parameters for $Ni_{5.62(1)}SnSe_2$ and $Ni_{5.78(2)}SnTe_2$

	Wyckoff	*x/a*	*y/b*	*z/c*	s.o.f.	U^{eq}
$Ni_{5.62(1)}SnSe_2$						
Sn	2(*a*)	0	0	0	1	0.0075(4)
Se	4(*c*)	1/2	1/2	0.18118(7)	1	0.0111(4)
Ni(1)	2(*b*)	1/2	1/2	0	1	0.0066(5)
Ni(2)	8(*g*)	0	1/2	0.10100(7)	1	0.0083(3)
Ni(3)	4(*c*)	0	0	0.1985(3)	0.309(7)	0.011(1)
$Ni_{5.78(2)}SnTe_2$						
Sn	2(*a*)	0	0	0	1	0.0084(3)
Te	4(*c*)	1/2	1/2	0.18150(5)	1	0.0096(3)
Ni(1)	2(*b*)	1/2	1/2	0	1	0.0086(5)
Ni(2)	8(*g*)	0	1/2	0.09403(7)	1	0.0100(3)
Ni(3)	4(*c*)	0	0	0.1904(3)	0.39(1)	0.012(1)

patterns showed all samples to contain Ni as the only impurity.

2.4. Electronic structure and bonding

The electronic structures of model compounds $Ni_{5.75}SnSe_2$ and $Ni_{5.75}SnTe_2$ were calculated by use of the CRYSTAL98 [6] program package. Hay–Wadt effective core potentials (ECPs) and valence basis sets [7] modified for the calculation of solids, in accordance with recommendations of CRYSTAL98 manual, were used in the calculations employing the B3LYP Hamiltonian. The basis sets were tested in the calculations of metals and binary chalcogenides and were found to be suitable for adequate representation of the main features of their electronic structure and bonding. The convergence criterion for the SCF energy was set to 10^{-7} Hartree. The basis sets and atomic coordinate sections of CRYSTAL98 input files are available in the Supporting Information. Difference charge density plots obtained by the use of TOPOND98 [8] and gOpenMol [9] software were analyzed in order to reveal the main features of chemical bonding as described in [2,10,11].

3. Results and discussion

3.1. Electron diffraction

The ED pattern for $Ni_{5.78}SnTe_2$ are presented in Fig. 2. The brightest spots in all reciprocal space sections correspond to the average structure with tetragonal $I4/mmm$ symmetry. However, the satellite reflections observed on the $[\bar{1}01]^*$ and $[\bar{4}01]^*$ patterns can be indexed with the modulation vector $\mathbf{q} \approx 0.4\mathbf{a}^*$. Thus, the crystal structure is modulated and evidently has a lower symmetry than the tetragonal, presumably orthorhombic. Since the ordering along *a* or along *b* dimensions is equiprobable due to similarity of unit cell parameters *a*

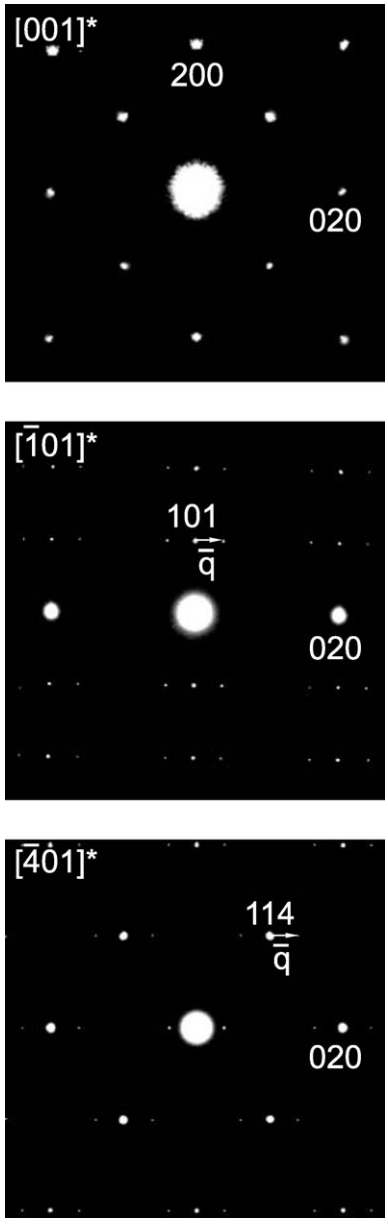

Fig. 2. $[001]^*$, $[\bar{1}01]^*$ and $[\bar{4}01]^*$ ED patterns of $Ni_{5.78}SnTe_2$.

and b we can suppose coherent twinning of crystals. Crystal structure refinement within $(3+n)D$ higher dimension formalism and detailed description of modulated structure, as well as results of ED experiments for $Ni_{5.62}SnSe_2$, will be reported further.

3.2. Average crystal structure

The crystal structures of the title compounds were found to be very close to those of the nickel-antimony selenide and telluride ($Ni_{5.72}SbSe_2$, $Ni_{5.66}SbTe_2$) reported earlier [1]. The average crystal structures are made by heterometallic $^2_\infty[Ni_5Sn]$ slabs of Cu_3Au type and nickel-chalogenide $^2_\infty[Ni_xQ_2]$ (Q=Se, $x=0.62$; Q=Te, $x=0.78$) slabs of distorted NaCl type with partially occupied Ni(3) sites. These slabs alternate along the crystallographic c-axis (Fig. 3). The shortest interatomic distances are listed in Table 4.

The Ni–Sn distances are close to those observed in Ni_3Sn [6] (2.648 Å) and $Ni_3Sn_2S_2$[12] (2.70–2.73 Å). The Ni–Ni distances are slightly longer as compared to those in metallic Ni [13] (2.49 Å). The Ni–Te distances in $Ni_{5.78}SnTe_2$ are close to those in $Ni_{2.86}Te_2$ [14] or NiTe [15] (2.42–2.65 Å). The shortest Ni–Se distances are a bit shorter than those in binary selenides (cf. 2.29–2.5 Å in Ni_3Se_2 [16], and the shortest is 2.287 Å in Ni_6Se_5 [17]). A similar situation was observed in the nickel–antimony selenide [1] and nickel–tin sulfides [2]. Other interatomic separations are longer than 3.6 Å and should be considered as nonbonding.

One of the simplest possible models of the $Ni_{5.75}SnSe_2$ average crystal structure, where only $\frac{3}{8}$ of the Ni(3) sites

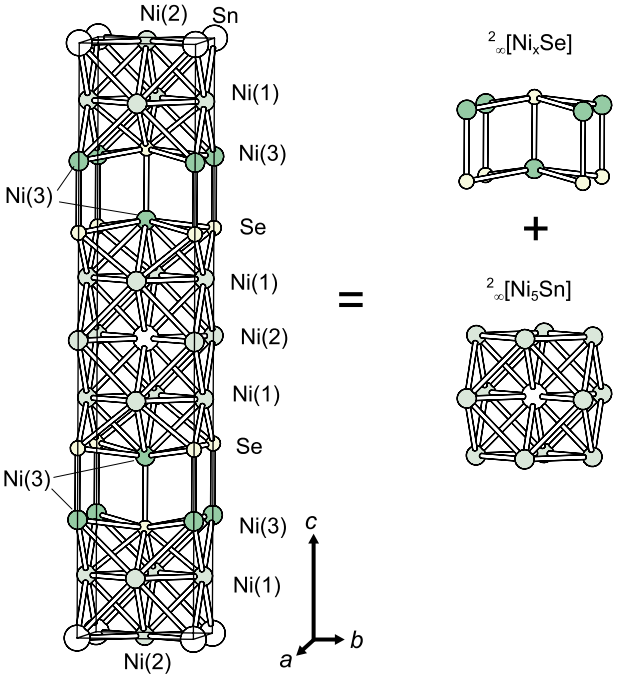

Fig. 3. The crystal structure of $Ni_{5.62}SnSe_2$.

Table 4
Interatomic distances in $Ni_{7-\delta}SnQ_2$ (Q = Se, Te)

	$Ni_{5.62}SnSe_2$ (Å)	$Ni_{5.78}SnTe_2$ (Å)
Ni(1)–Ni(1)	2.6085(6)	2.6644(4)
Ni(1)–Ni(2)	2.6362(9)	2.624(1)
Ni(1)–Ni(3)	2.589(4)	2.658(4)
Ni(1)–Sn	2.6362(9)	2.624(1)
Ni(2)–Sn	2.6085(6)	2.6644(4)
Ni(1)–Q	2.374(1)	2.536(1)
Ni(3)–Q	2.245(6), 2.6283(9)	2.484(6), 2.6703(5)

are occupied is illustrated in Fig 4. Due to that partial occupation, the crystal structures of the title compounds can be described as constructed from thick sheets of the height of about 6 Å terminated by surprisingly few Ni–Q bonds. Since, the number of bonds inside and between the thick sheets differ significantly, strong anisotropy of the physical properties of those compounds should be expected.

3.3. Physical properties

3.3.1. Thermal properties

The pure substances were placed in small quartz ampoules, which were evacuated and sealed. The differential thermal analysis curves were registered in the heating mode (10°C/min heating rate).

$Ni_{5.62}SnSe_2$. Three resolved endothermic effects (at 239 ± 5°C, 742 ± 5°C and 825 ± 5°C) were registered. The first effect (239°C) probably corresponds to a solid phase transition and not to decomposition, because the single crystals of $Ni_{5.62}SnSe_2$ were successfully grown at higher temperatures (about 560°C). The two other effects may correspond to peritectical melting of the substance, since solidified melt was observed after cooling and further X-ray powder analysis of the ground melt showed the presence of $Ni_{5.62}SnSe_2$, Ni_3Sn and Ni_3Se_2.

$Ni_{5.78}SnTe_2$. Four resolved endothermic effects (at 781 ± 5°C, 913 ± 5°C, 977 ± 5°C and 997 ± 5°C) were registered. The first effect at 781°C probably corresponds to a solid phase transition. In order to confirm this hypothesis the sample was quenched from the temperature slightly above that to cold water. Its X-ray powder pattern showed only few additional weak (less than 1% intensity) reflections. The other effects probably correspond to solid state transitions and the ultimate decomposition of $Ni_{5.78}SnTe_2$, since the cooled sample showed no signs of being molten and its X-ray powder pattern indicated the presence of $Ni_{5.78}SnTe_2$, Ni_3Sn and $Ni_{2.86}Te_2$.

3.3.2. Electrical properties

The pure substances were pressed into rectangular ($2\times3\times2$ mm) pellets. The resistivities of those pellets

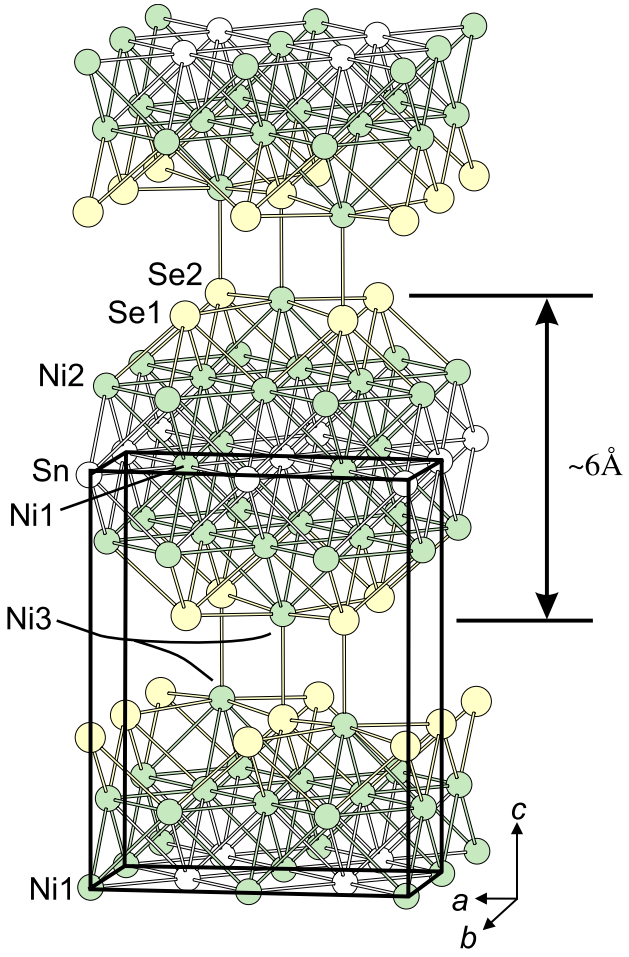

Fig. 4. The unit cell of the ordered model $Ni_{5.75}SnSe_2$. Enveloped is the part of the unit cell used in the analysis of the $\Delta\rho$ maps (see below).

were measured orthogonal by (for both $Ni_{5.62}SnSe_2$ and $Ni_{5.78}SnTe_2$) and along (for $Ni_{5.62}SnSe_2$ only, because the telluride pellet was very fragile and destroyed after the first measurement) the direction of load applied in the temperature range 4.2–300 K employing the standard four-probe technique by using silver paste contacts.

The temperature dependence of the resistivity of $Ni_{5.62}SnSe_2$ measured in the parallel ($\rho_{||}$) or orthogonal ($\rho_{\perp}$) direction of compression is shown in Fig. 5a. Fig. 5b displays the temperature dependence of resisitivity for $Ni_{5.78}SnTe_2$ measured in the orthogonal direction of compression. According to this data, the resisitivity decreases when temperature decreases, which is the characteristic feature of the metal.

In the interpretation of resistivity data, it is assumed that the observed anisotropy of resistance of $Ni_{5.62}SnSe_2$ is caused by the anisotropy of the low-dimensional crystal structure. Mechanical compression is thought to lead to a preferred orientation of small crystallites in the pellet, as confirmed by X-ray data (DRON-4 powder diffractometer, 0.1° 2θ step, graphite monochromator, scintillation counter; Fig. 6). The top diffraction pattern shows the peaks of (00l) planes to be the strongest, while the same peaks are weaker in the bottom diffraction pattern. This observation supports the above hypothesis, since it indicates that small crystals in the pellet after compression are oriented so that their crystallographic c axes to a large extent are parallel to the direction of compression, and consequently the (00l) planes end up being almost perpendicular to it.

3.3.3. Magnetic properties

Pure $Ni_{5.78}SnTe_2$ and $Ni_{5.62}SnSe_2$ powders were pressed into rectangular pellets ($5\times10\times3$ mm) from which a small piece ($2\times3\times2$ mm) was cut by electro-erosion technique. The dependences of the magnetic moment P_m on temperature in the temperature range 4.2–300 K were registered by Sample Vibrating Magnetometer PARC-155 (Princeton, USA) with temperature regulation by PARC-152 in Cryostat PARC-153. Fig. 7 shows the temperature dependence of product χT for $Ni_{5.78}SnTe_2$ (a) and $Ni_{5.62}SnSe_2$ (b). Experimental data may be approximated by dependence $\chi=\chi_0+C/(T+\theta)$ where $\chi_0=2.96\times10^{-6}$ emu/g Oe (4.74×10^{-6}), $C=7.90\times10^{-5}$ emu K/g Oe (10.4×10^{-5}) and $\theta=+3.6$ K (6.3) for $Ni_{5.78}SnTe_2$ ($Ni_{5.62}SnSe_2$) (solid lines in Fig. 7).

The temperature-independent term can be attributed to either Pauli or van Vleck paramagnetism of mixed nickel–tin selenide or telluride. The former suggestion is confirmed by the results of theoretical calculations (see below).

The local magnetic moment μ of Curie–Weiss contribution can be evaluated using the experimental value of $C=\mu^2/3k$. The calculated value of μ per formula unit is equal to $0.630\mu_B$ (for $Ni_{5.78}SnTe_2$ sample). The magnetic moment of Ni in metal state at $T=0$ K is equal to $0.6157\mu_B$. The magnetic moment of Ni^{+2} ion under orbital freezing is equal to $2.83\mu_B$ or $5.59\,\mu_B$ in unfrozen state (Russel–Saunders approximation). Curie–Weiss contribution in both samples can be assigned either to paramagnetic impurities (nickel chalcogenides) or to the presence of localized magnetic moments on Ni atoms in mixed nickel–tin selenide or telluride. The former suggestion is confirmed by theoretical calculation results (see below), showing complete filling of Ni d-bands and thus the absence of localized magnetic moments in $Ni_{5.75}SnQ_2$ (Q=Se, Te). A small amount of paramagnetic impurity is not visible on X-ray powder patterns.

3.4. Electronic structure and bonding

Because of the presence of the partially occupied site Ni(3) in both compounds, an ordering model needs to be proposed in order to perform band structure calculations. We decided to use a model based on the composition $Ni_{5.75}SnQ_2$ and the s.o.f. of Ni(3) site equal to 0.375. This results in a unit cell 4 times bigger because

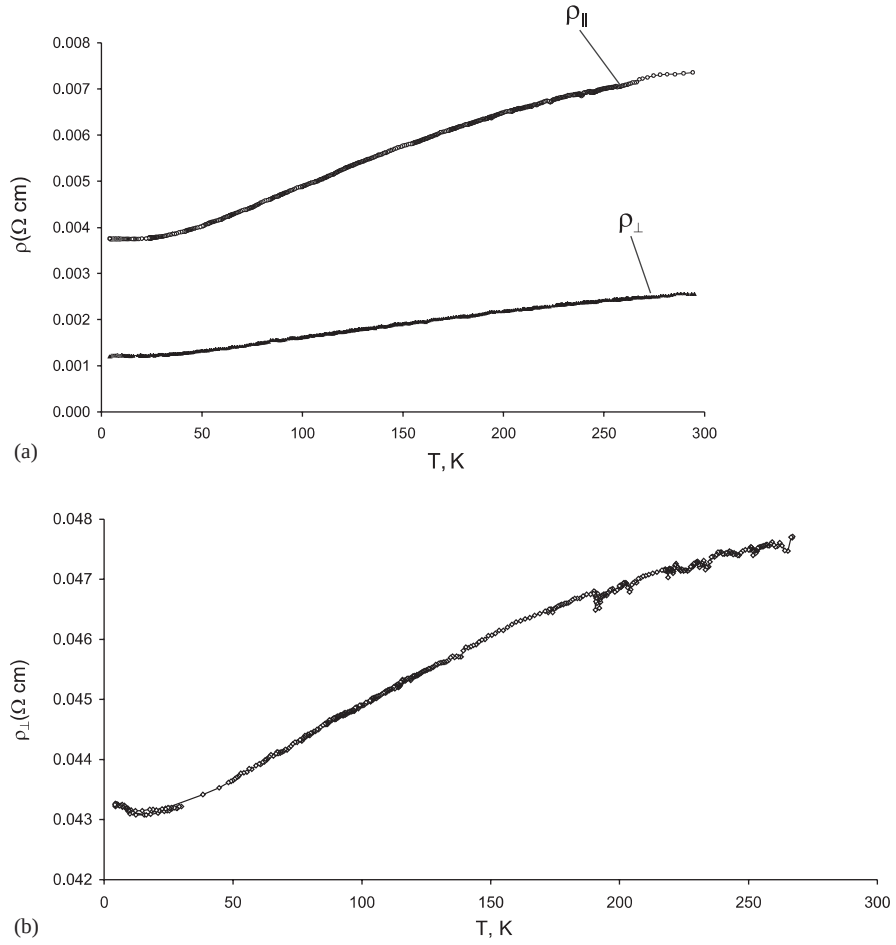

Fig. 5. Resistivity of $Ni_{5.62}SnSe_2$ (a) and $Ni_{5.78}SnTe_2$ (b) pressed pellets measured along ($\rho_{||}$) and orthogonal ($\rho_{\perp}$) to the pellet load direction.

of the necessary doubling of the crystallographic *a* and *b* axes. The vacancies are arranged so that as much symmetry as possible is retained, including the inversion center (Fig. 4).

The model unit cell used in the calculations is shown in Fig. 4. Part of the cell, enveloped by a solid line, was used in an analysis of the difference charge density, since it contains all unique atoms and interactions.

The calculation results for $Ni_{5.75}SnSe_2$ and $Ni_{5.75}SnTe_2$ were found to be very similar, and consequently our subsequent discussion is focused on the selenium compound, unless otherwise stated.

The calculated density of states (DOS) are shown in Fig. 8. All atomic states are strongly mixed and there are essentially no peaks having a dominant contribution from only one type of atom. Disregarding the difference in coordination, it can be noted that, the states of nickel atoms from the heterometallic slabs $^{2}_{\infty}[Ni_5Sn]$ are located in essentially same energy range as those from the chalcogenide blocks. Another interesting fact is that in addition to Se *sp*-states the Ni *d*-states are almost fully occupied, while tin *p*-states are only partially occupied. This is compliant with the Mulliken charge distribution: Sn: +0.7, Se: −1, the charges of Ni atoms vary from close to zero for those in the middle of heterometallic slabs to +0.2 for Ni atoms inside the chalcogenide blocks. Consequently, one may suggest that Se atoms withdraw electron density from Ni atoms and, in turn, Ni atoms withdraw the electron density from tin atoms. A similar tendency was previously observed in nickel–tin sulfides [2] and mixed scandium tellurides [18].

The band structure of $Ni_{5.75}SnSe_2$ in the vicinity of the Fermi level is shown in Fig. 9. Two-dimensional metallic conductivity is obvious because in the Γ–Z direction the Fermi level resides in the energy gap, in contrast to the orthogonal Γ–X–M directions. The low DOS at the Fermi level (Fig. 8) suggests that the compound exhibits Pauli paramagnetic behavior.

Fig. 10 shows the difference charge density in the part of the model unit cell marked in Fig. 4. The left picture, where the isosurface of level $+0.0156\,e\,a.u.^{-3}$ is represented, reveals the strongest type of interaction; isosurfaces with smoothed tetrahedral shape are labelled A.

These correspond to 4-center, 3Ni + Sn interactions and reside in the center of nearly regular $[Ni_3Sn]$

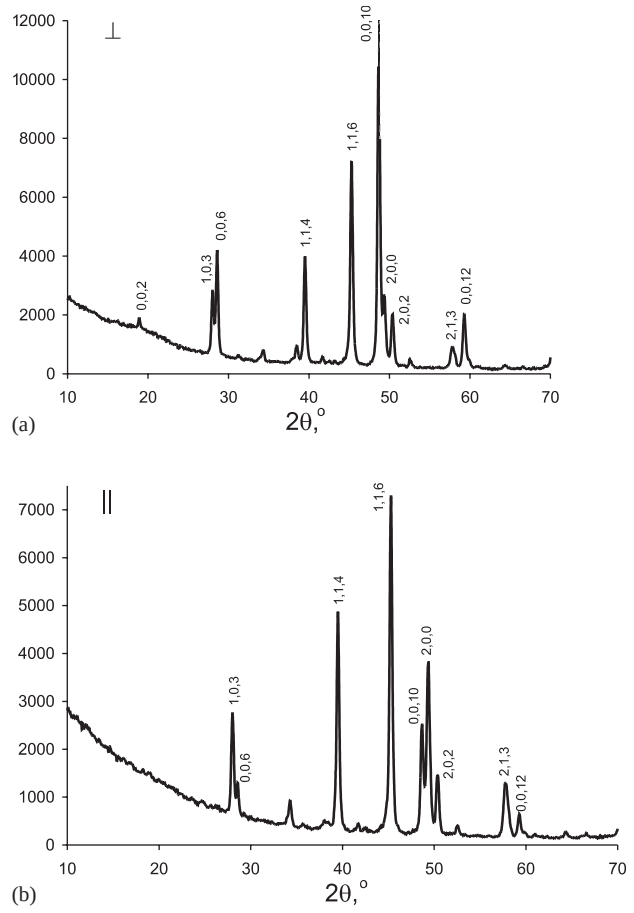

Fig. 6. Diffraction patterns taken from two different faces of a compressed $Ni_{5.62}SnSe_2$ pellet—orthogonal to the direction of compression (a) and parallel to it (b).

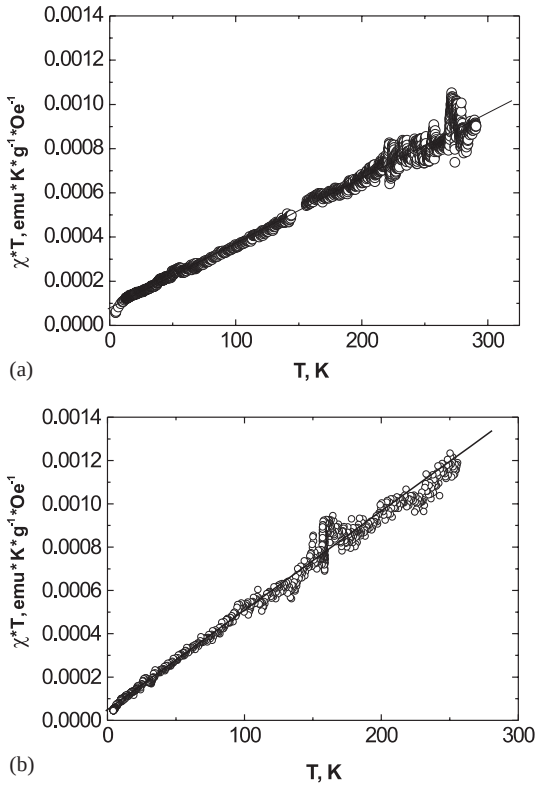

Fig. 7. Temperature dependencies of product χT for $Ni_{5.78}SnTe_2$ in magnetic field 3043.3 Oe (a) and $Ni_{5.62}SnSe_2$ in magnetic field 1517 Oe (b).

tetrahedra in the nickel–tin bimetallic slab. The spherical isosurfaces labelled B correspond to 4-center, 3Ni + Se (B) interactions. This interaction binds the bimetallic and nickel–selenide slabs together.

The interactions within the nickel–selenide slabs in $Ni_{5.75}SnSe_2$ seem to be weaker than those described above, since the $\Delta\rho$ level has to be decreased to $+0.009\,e\,a.u.^{-3}$ in order to reveal it's the relevant isosurfaces, labelled C in Fig. 10. These are interpreted as pairwise Ni–Se interactions.

4. Conclusion

The title compounds and the recently obtained and characterized mixed nickel-antimony selenide and telluride [1] and nickel–tin sulfides [2] form a new class of compounds with characteristic slab structures. The average crystal structures of the title compounds are made from the same type of blocks as those in $Ni_{7-\delta}SbQ_2$ (Q=Se, Te) and strongly resemble the structure of Ni_6SnS_2. The comparison of mixed nickel–tin and nickel–antimony chalcogenides crystal structures shows a slight decrease of the a unit cell parameter and slight increase of the c parameter, while antimony substitutes for tin (about 0.1–0.2 Å). Bond lengths and distortion angle within nickel-chalcogen slabs remain almost constant (see Table 4 for distance values, angles of distortion are Se–Ni(3)–Se) ≈ 97° and Te–Ni(3)–Te) ≈ 94°. This fact is probably caused by Sn and Sb metallic radii similarity (1.58 and 1.61 Å for CN = 12, consequently [19]). As no electronic structure calculations are presented in [1] we cannot compare changes caused by charge effects. The Ni(3) site occupancy differs significantly in pairs of selenides $Ni_{5.62}SnSe_2$ and $Ni_{5.72}SbSe_2$ and tellurides $Ni_{5.78}SnTe_2$ and $Ni_{5.66}SbTe_2$. Most likely these distinctions are caused by p-metal substitution and should be attributed to electronic effects rather than size factors.

It is interesting to note that nickel-chalcogenide slabs of Li_2O type were found only in the mixed nickel–tin sulfides, whereas rock-salt slabs exist in all compounds of the discussed type. Similarly, $^2_\infty[Ni_8Sn_2]$ double-packed slabs were also only found in the mixed sulfides. Possible explanation can be atom size factors, for example, originating from requirement of slab commensurability; however, electronic factors also could play a role.

Investigations of electrical properties measured along and perpendicular to the direction of compression

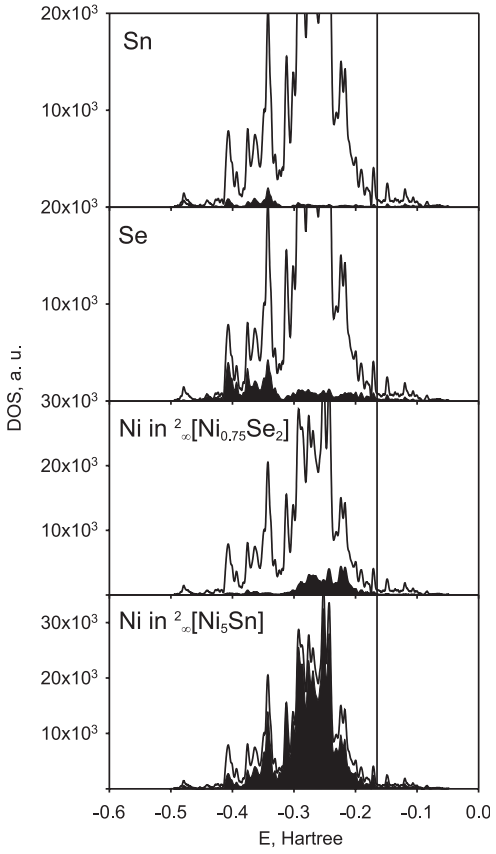

Fig. 8. The density of states for $Ni_{5.75}SnSe_2$.

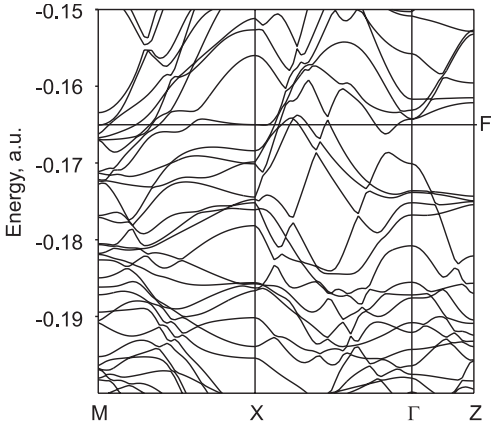

Fig. 9. The band structure of $Ni_{5.75}SnSe_2$.

revealed a strong anisotropy of physical properties, also displayed in the calculated band structure of $Ni_{5.62}SnSe_2$. This anisotropy is a direct consequence of the crystal structure of nickel–tin mixed selenide, assembled from two types of slabs with markedly different nature of chemical bonding, as highlighted by the difference charge density maps. At the same time, neither nickel–tin telluride nor nickel–tin suldifes have such well-pronounced anisotropy of their band structure, although the nature of chemical bonding in the

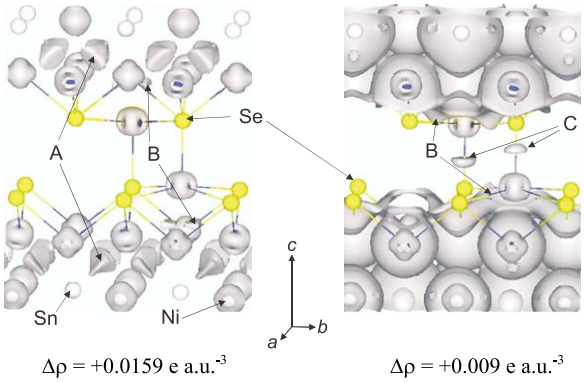

Fig. 10. Difference charge density distribution in $Ni_{5.75}SnSe_2$.

bimetallic and nickel-chalcogenide slabs also differs significantly in these compounds. The explanation may be attributed to the particular energy of Se atomic states, which result in a band gap in the Γ–Z direction to be formed.

The "electronic flexibility" of the bimetallic slabs and the possibility to combine it with various nickel-chalcogenide slabs may indicate that numerous other compounds of this type can be synthesized. Such studies are presently underway.

Acknowledgments

This work was supported by RFBR program (Grant 03-03-32831) and program Universities of Russia 2004 and by the Göran Gustafsson Foundation. The authors gratefully thanks A.V. Mironov and Dr. A.M. Abakumov for ED experiments and fruitful discussion.

Supporting Information Available: X-ray crystallographic file for $Ni_{5.62}SnSe_2$ and $Ni_{5.78}SnTe_2$ (CIF). Basis set and input coordinates used in the calculations of electronic structures with the CRYSTAL98 software.

References

[1] T.K. Reynolds, J.G. Bales, F.J. DiSalvo, Chem. Mater. 14 (2002) 4746–4751.
[2] A.I. Baranov, A.A. Isaeva, L. Kloo, B.A. Popovkin, Inorg. Chem. 42 (2003) 6667–6672.
[3] N.P. Lyakishev (Ed.), Phase Diagrams of Binary Metallic Systems. Mashinostroenie, Moscow, 1996.
[4] (a) G.M. Sheldrick, SHELXS-97, Program for crystal structure solution; University of Göttingen, Göttingen, Germany, 1997;
(b) G.M. Sheldrick, SHELXL-97, Program for crystal structure refinement; University of Göttingen, Göttingen, Germany, 1997.
[5] (a) SCALEPACK. KappaCCD Software. Nonius BV, Delft, The Netherlands, 1998;
(b) Z. Otwinowski, W. Minor, in: C.W. Carter Jr., R.M. Sweet (Eds.), Methods in Enzymology, Academic Press, New York, 1997, p. 276.

[6] V.R. Saunders, R. Dovesi, C. Roetti, M. Causa, N.M. Harrison, R. Orlando, C.M. Zicovich-Wilson, CRYSTAL98 User's Manual, University of Torino, Torino, 1998.
[7] (a) for Ni: F. Freyria-Fava, Thesis, Turin, 1997;
(b) P.J. Hay, W.R. Wadt, J. Chem. Phys. 82 (1) (1985) 284–298 (for Sn, Te).
[8] C. Gatti, TOPOND 98 User's Manual, CNR-CSRSRC, Milano, 1999.
[9] L. Laaksonen, gOpenMol, version 1.4: http://www.csc.fi/~laaksone/gopenmol/gIntro.html
[10] A.I. Baranov, L. Kloo, A.V. Olenev, B.A. Popovkin, A.I. Romanenko, A.V. Shevelkov, J. Am. Chem. Soc. 123 (2001) 12375–12379.
[11] A.L. Lyubimtsev, A.I. Baranov, A. Fischer, L. Kloo, B.A. Popovkin, J. Alloys. Compd. 340 (2002) 167–172.
[12] K.-J. Range, F. Rau, M. Zabel, H. Paulus, Z. Kristal. 212 (1997) 50.
[13] H.E. Swanson, E. Tatge, Natl. Bur. Stand. (US) Circular 539 (1953) 1–95.
[14] R.B. Kok, G.A. Wiegers, F. Jellinek, Recl. Trav. Chim. Pays-Bas Belg. 84 (1965) 1585–1588.
[15] K.O. Klepp, K.L. Komarek, Monatsh. Chem. 103 (1972) 934–946.
[16] J.P. Rouche, P. Lecocq, C R Hebdomad. Seances Acad. Sci. C Sci. Chimiq. 262 (1966) 555–556.
[17] E. Rost, K. Haugsten, Acta Chem. Scand. 25 (1971) 3194–3196.
[18] L. Chen, J.D. Corbett, Inorg. Chem. 41 (2002) 2146–2150.
[19] A.F. Wells, Structural Inorganic Chemistry, Clarendon Press, Oxford, 1945.